Computational Analysis of Wave and Current Interactions with Mangrove Forests

Wen-Huai Tsao[1,2] and Chris Kees[2,3]
[1]Coastal Ecosystem Design Studio, Louisiana State University, Baton Rouge, LA; [2]Department of Civil and Environmental Engineering, Louisiana State University, Baton Rouge, LA;
[3]Center for Computation and Technology, Louisiana State University, Baton Rouge, LA

LSU Department of Civil & Environmental Engineering

LSU Center for Computation & Technology

Introduction

Natural-based structures are essential solutions to storm protection, ecosystem restoration, and shoreline stabilization. Field and laboratory studies have provided several empirical equations for computing hydrodynamic drag and estimating wave attenuation, while numerical methods can simulate the effects of critical wave impact on various coastal environments, without paying massive cost and manpower. Consequently, the need for reliable numerical methods is fundamental for ecosystem design and hazard assessment. This research focuses on implementing a high-order phase-resolving Cut Finite Element Method (CutFEM) for the multiscale analysis of waves/currents interacting with mangrove forests to support the engineering design of resilient shorelines. All numerical modules are implemented by *Proteus* (https://proteustoolkit.org/).

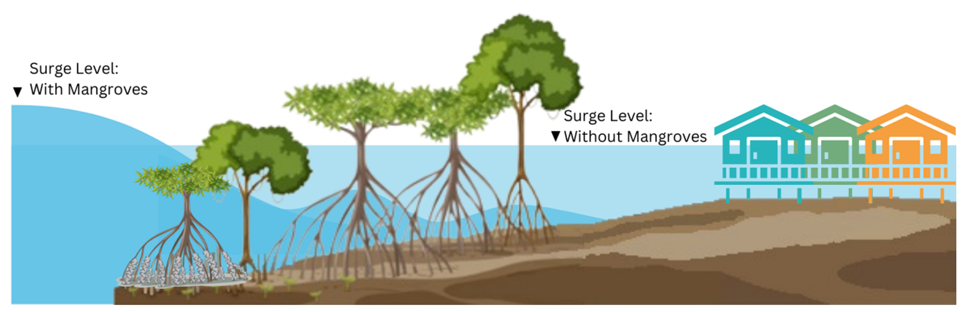

Hybrid LS-VOF Method for Navier-Stokes Flow

For a fluid domain consisting of two incompressible Newtonian phases, i.e., air and water, separated by a sharp material interface, the continuity and Navier-Stokes equations are:

$$\nabla \cdot \boldsymbol{u} = 0 \tag{1}$$

$$\rho[\partial_t \boldsymbol{u} + (\boldsymbol{u}\cdot\nabla)\boldsymbol{u}] - \nabla\cdot\boldsymbol{\sigma} = \boldsymbol{f} \tag{2}$$

where $\partial_t = \frac{\partial}{\partial t}$, ρ is the density, $\boldsymbol{u}$ is the fluid velocity, $\boldsymbol{\sigma} = -p\boldsymbol{I} + 2\mu\nabla\boldsymbol{u}$, μ is the viscosity, and $\boldsymbol{f}$ is the body forces per unit mass. Based on the assumption of continuity of velocity and stress, the boundary conditions on the air-water interface can be written as:

$$p_w = p_a, \boldsymbol{u}_w = \boldsymbol{u}_a, \boldsymbol{\sigma}_w\cdot\boldsymbol{n} = \boldsymbol{\sigma}_a\cdot\boldsymbol{n} \tag{3}$$

Note that the subscripts w and a denote the water and air phases, respectively. Kees et al. [1] proposed the weak variational form of phase conservation to build a hybrid LS-VOF scheme without excessive mass loss or smearing of the interface. Quezada de Luna et al. [2] reformulated a monolithic equation to provide local mass conservation and signed distance property. The projection scheme is used to ensure second-order accuracy in space. When the mesh is refined, this extra viscosity must vanish.

Implementation of CutFEM

To solve multi-phase Navier-Stokes flow with embedded solid interfaces, boundary-conforming FEMs were proposed to facilitate the application of boundary conditions. The CutFEM "cuts" meshes to fit the solid interfaces that are not mesh-conforming. Kees et al. [3] employed the equivalent polynomial to obtain the high-order accuracy in the numerical integrals along the cut cell. Their method not only ensures robustness but also upgrades legacy codes easily. For the two-phase domain shown in Fig. 1(a), let ϕ_s be the solid level set function that represents Γ_s through ϕ_s=0, hence,

$$\phi_s = \begin{cases} d_E, & \boldsymbol{x}\in\Omega_f \\ -d_E, & \boldsymbol{x}\in\Omega_s \end{cases} \tag{4}$$

where d_E is the Euclidean distance from a point to the interface Γ_s. Fig. 1(b) shows the linear discretization of the phase geometry with triangle meshes cut by Γ_s. Note that it can only be cut once. Since the motion of the solid phase $\boldsymbol{u}_s$ is assumed to be known, the no-slip boundary condition at the fluid-solid interface can be written as:

$$\boldsymbol{u} = \boldsymbol{u}_s, \mathrm{on}\Gamma_\mathrm{s} \tag{5}$$

Nitsche's Method is applied to ensure flux conservation in the discrete weak formulation. Therefore, the Dirichlet condition becomes:

$$\int_{\Gamma_s} k\nabla\boldsymbol{u}\cdot\boldsymbol{n} + \frac{C}{h}(u-u_s) = \int_{\Omega_s} f \tag{6}$$

where C is a numerical parameter. By using Eq. (6), the flux across the embedded boundary can be directly calculated. The pressure and velocity jump penalties are used in the discrete weak formulation to enhance stability and bound the condition number independent of the location of the cut surface. Therefore,

$$\int_{\Omega_f} H(\phi_s)[\rho(\partial_t\boldsymbol{u}\partial_t + \boldsymbol{u}\cdot\nabla\boldsymbol{u} - \boldsymbol{f})\boldsymbol{w} + \sigma:\nabla\boldsymbol{w}]d\Omega + \int_{\Omega_f}\delta(\phi_s)[\sigma\boldsymbol{n}_s\boldsymbol{w} + (\boldsymbol{u}-\boldsymbol{u}_s)\sigma\boldsymbol{n}_s + \frac{C\mu}{h}(\boldsymbol{u}-\boldsymbol{u}_s)\boldsymbol{w}]d\Omega + s_u + g_u = 0 \tag{7}$$

$$\int_\Omega H(\phi_s)\boldsymbol{u}\cdot\nabla w + \int_\Omega \delta(\phi_s)\boldsymbol{u}_s\cdot\boldsymbol{n} + s_p + g_p = 0 \tag{8}$$

where s and g with subscripts u and p are consistent stabilization and ghost penalty terms for velocity and pressure, respectively.

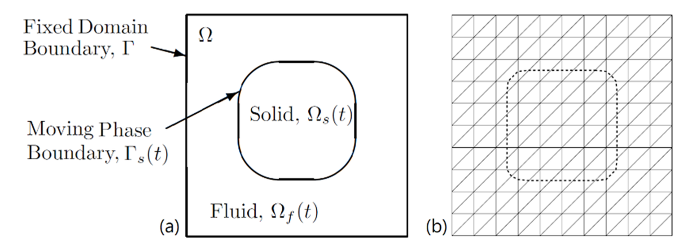

Figure 1: Computational domains and boundaries: (a) fixed domain Ω and boundary Γ with two dynamic subdomains, Ω_s and Ω_f, and phase boundary Γ_s, (b) piecewise linear phase boundary (dashed line) from zero level set.

Experiments of Wave Attenuation by Mangrove Forests

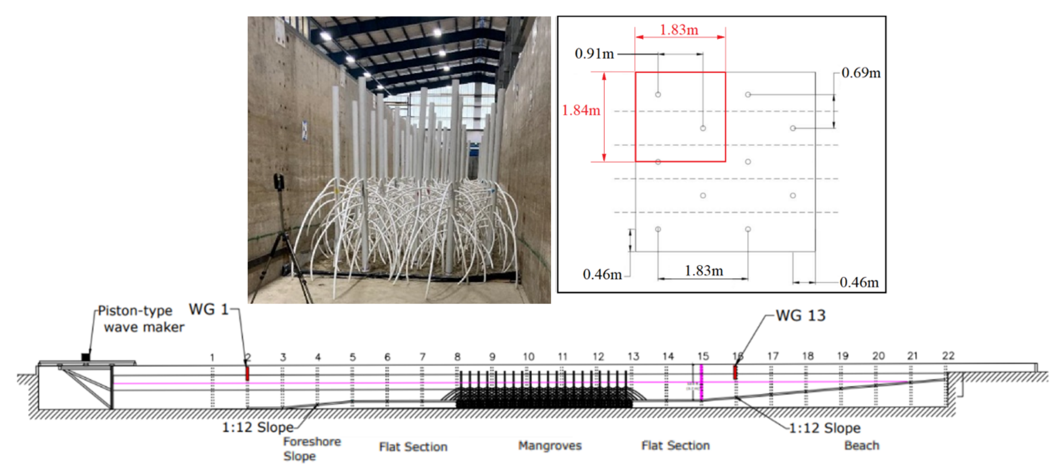

Figure 2: The numerical methods are validated by experiments of wave attenuation through mangrove forests [4]. Several PVC trunk-root units were arranged randomly to mimic a real mangrove forest. The regular and random waves were tested by utilizing airy wave theory and the JONSWAP spectrum, respectively. The wave elevations at thirteen wave gauges distributed along the flume were compared to examine the wave attenuation due to mangrove forests.

Volume-Averaging Hydrodynamic Analysis

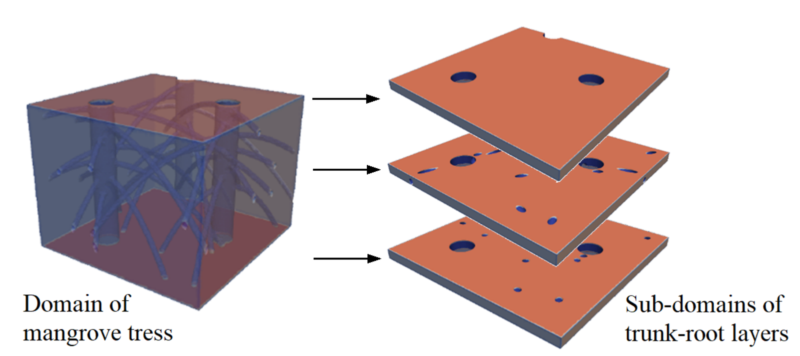

Figure 3: The momentum dissipation due to mangrove forests is assumed to depend on the projected area of the trunk-root model on the plane perpendicular to the flow. Since the projected area changes along the vertical direction, the numerical domain is divided into a stack of sub-domains. We employ a volume-averaging method to separately analyze the hydrodynamic drag caused by different layers of the prop root structure. This approach doesn't require additional tuning parameters or experimental measurement but also avoids the excessive computational cost of refining mesh around the roots. Note that considering the symmetry of the layout of the mangrove forests, only one subdivision (red square in Fig. 2) will be used in the characteristic analysis.

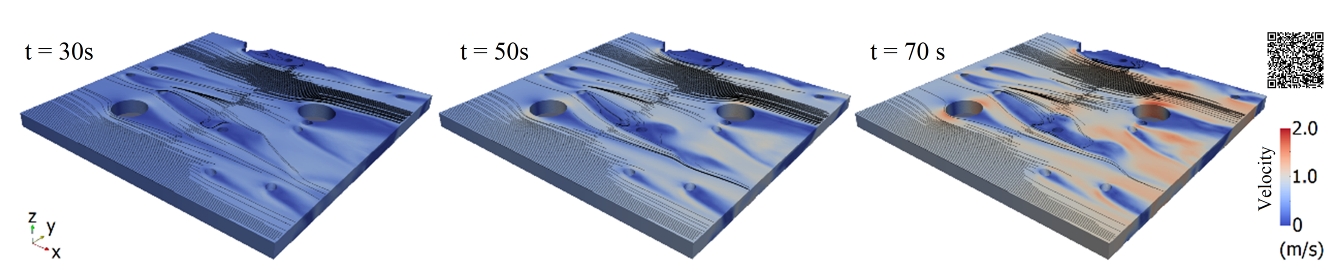

Figure 4: For the fluid field in the bottom sub-domain, the velocity magnitude around and behind the trunks and roots decreases significantly. Wakes are observed. The plot of streamlines doesn't show that strong vortex shedding when fluid velocity is slow as input velocity increases. No significant transverse component is observed.

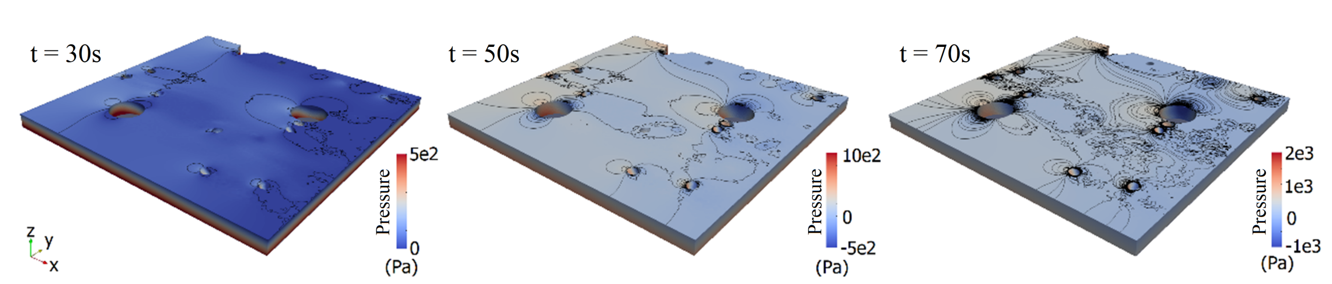

Figure 5: For the fluid field in the bottom sub-domain, the front roots are subject to higher pressure, while the lower pressure forms in the area behind the roots. The contour lines are perpendicular to the flow direction, meaning the average pressure along the flow direction drops consistently.

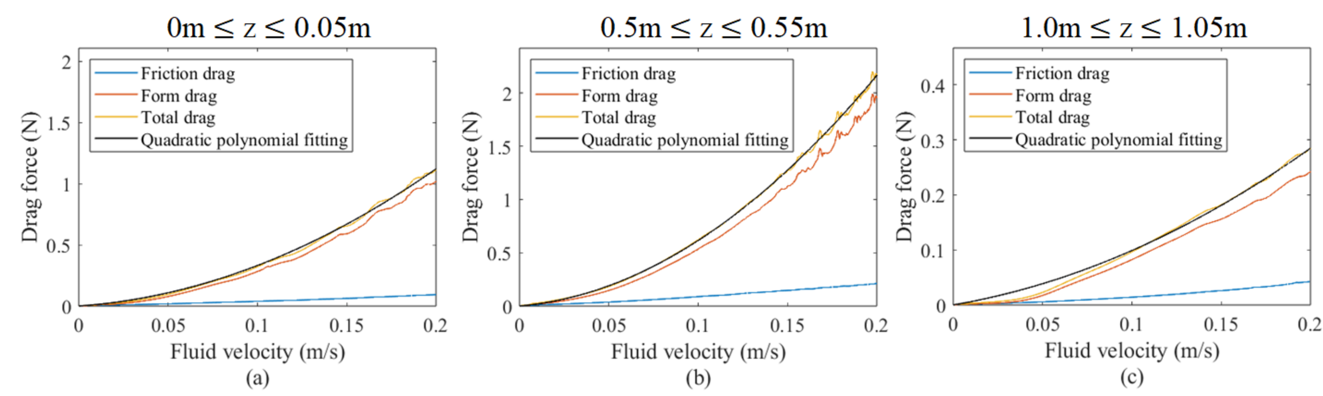

Figure 6: The drag by the trunk-root system can be computed by:

$$D = D_{form} + D_{friction} = \rho_w \int_{S_e} -p\boldsymbol{n}dS + \rho_w\int_{S_e}\mu\boldsymbol{n}\cdot\left(\nabla\boldsymbol{u} + \nabla\boldsymbol{u}^T\right)dS \tag{11}$$

where S_e is the fluid-solid interface. Note that D_{form} and $D_{friction}$ represent the form drag due to pressure anomalies and the friction drag due to fluid viscosity, respectively. The numerical results show that the total drag can approximated by a quadratic polynomial of the fluid velocity (disregarding the flow direction) expressed by:

$$D = \alpha|\boldsymbol{u}| + \beta|\boldsymbol{u}|^2 \tag{12}$$

Note that the constant term of the regression curve is ignored to satisfy zero force is created when $\boldsymbol{u}$ = 0.

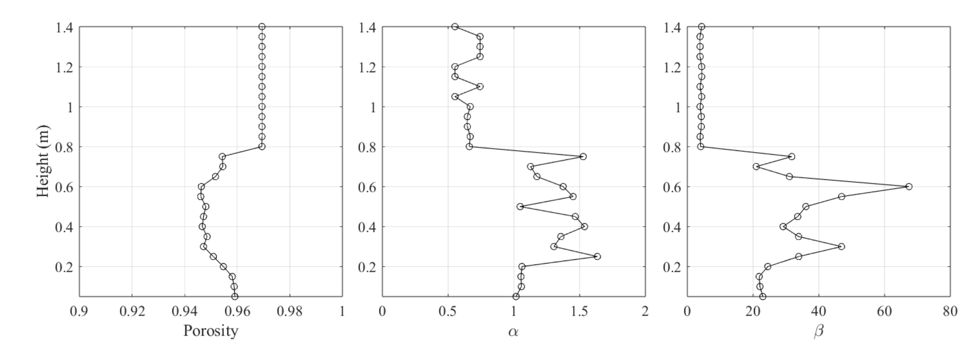

Figure 7: The drag coefficients α and β of each sub-domain are obtained by the volume-averaging method. The same amount of damping caused by the artificial mangrove forests can be produced by setting a numerical porous zone based on the Darcy-Forchheimer flow assumption expressed as:

$$\rho(\partial_t\boldsymbol{u} + \boldsymbol{u}\cdot\nabla\boldsymbol{u} - \boldsymbol{g}) - \nabla\cdot\boldsymbol{\sigma} = \nabla p_d = \alpha\boldsymbol{u} + \beta|\boldsymbol{u}|\boldsymbol{u} \tag{14}$$

The drag coefficients are not positively related to porosity. They cannot be solely determined by a single equation of any non-dimensional quantities. Therefore, the present approach provides an alternative solution for quantitative analysis.

Numerical vs Experimental Wave Elevations

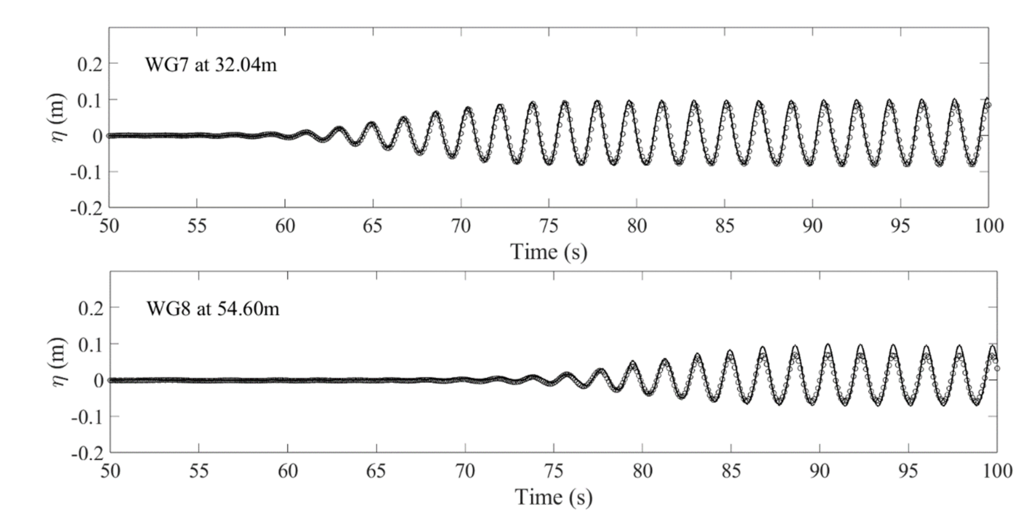

Figure 8: For the regular wave case, the numerical results are in good agreement with the experimental measurements. The strong damping decouples the nonlinear waves and dissipates their energy soon. The numerical model can deliver the accurate damping effect as the experimental model without using the drag coefficients measured in the experiments. Hence, it avoids massive fieldwork.

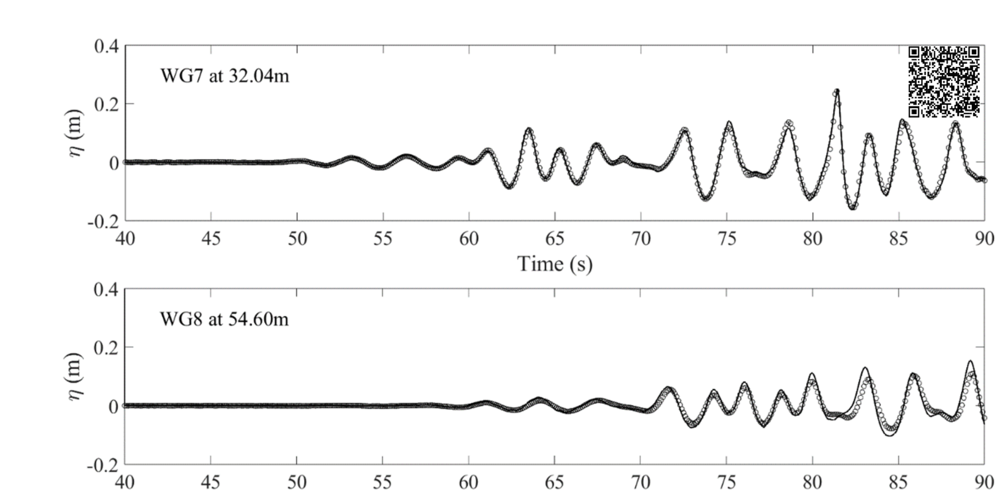

Figure 9: For the random wave case, some errors occur downstream (area behind the mangrove section) at the beginning of the simulation, but they vanish as the responses become steady. The wave attenuation is observed. Additionally, the wave speed decreases due to the resistance of the porous structure, hence, phase lag occurs. In general, the simplified model effectively predicts the total hydrodynamic resistance and global damping effectively.

Characteristics of Waves around Mangrove Trees

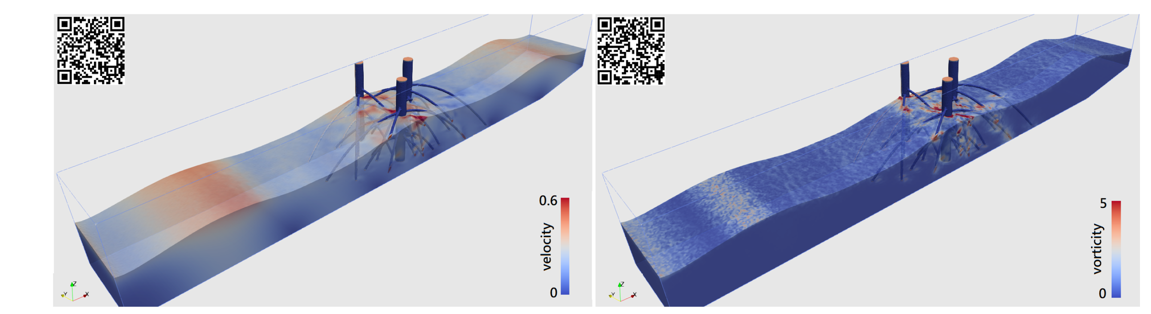

Figure 10: A numerical simulation incorporating the complete model of mangrove trees is conducted to analyze the wave field. As waves form, the wave crest exhibits higher velocity, with negligible vorticity. When it arrives at the mangrove area, high vorticity is generated in the vicinity of the roots, attenuating the fluid energy and consequently reducing the downstream wave velocity. The full simulation demonstrates comparable flow characteristics in the major direction (+x) to the volume-averaging approach. Therefore, the volume-averaging approach is approved as a viable alternative in cases of limited computational resources.

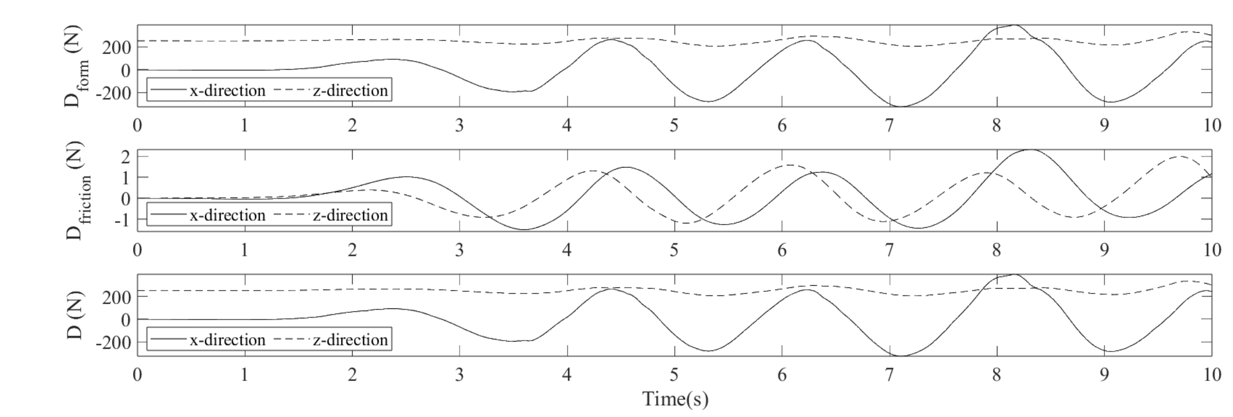

Figure 11: In the x-direction, the form drag undergoes oscillations synchronized with the wave motion. In the z-direction, the primary factor contributing to form drag is the hydrostatic effect, with dynamic drag playing a minor role. Friction drag, in comparison to form drag, is of lesser significance. A 90° phase lag exists between the x- and z-components, aligning with the wave motion. The full simulation offers the advantage of computing various components of drag without being confined to the assumption of homogeneity. This enables the extension of the simulation to incorporate a flexible trunk-root system.

Future Work

Future research will incorporate LiDAR scanning of actual mangrove trees into a numerical wave tank, enabling a thorough design analysis and assessment of storm and hurricane damage mitigation along the southern US coast. This research will be the foundation of the digital twin of coastal ecosystems.

References

[1] Kees, C.E., Akkerman, I., Farthing, M.W. and Bazilevs, Y. (2011). A conservative level set method suitable for variable-order approximations and unstructured meshes. *Journal of Computational Physics*, 230(12), 4536-4558.

[2] Quezada de Luna, M., Kuzmin, D., Kees, C.E. (2019). A monolithic conservative level set method with built-in redistancing. *Journal of Computational Physics*, 379, 262-278.

[3] Kees, C.E., Collins, J.H., Zhang, A. (2022). Simple, accurate, and efficient embedded finite element methods for fluid-solid interaction. *Computer Methods in Applied Mechanics and Engineering*, 389(1), 114404.

[4] Kelty, K.M., Tomiczek, T., Cox, D., Lomonaco, P., Mitchell, W. (2022). Prototype-scale physical model of wave attenuation through a mangrove forest of moderate cross-shore thickness: LiDAR-based characterization and Reynolds scaling for engineering with nature. *Frontiers in Marine Science*, 8, 780946.